Ocean Engineering, Volume 310, Part 2, October 2024, Article number 118760
DOI:10.1016/j.oceaneng.2024.118760

Motion response and energy harvesting of multi-module floating photovoltaics in seas

Zhi Zheng[b], Peng Jin[b], Qiang Huang[c], Binzhen Zhou[a, b, *], Ruoxuan Xiang[d], Zhaomin Zhou[d], Luofeng Huang[e]

[a] *State Key Laboratory of Subtropical Building and Urban Science, South China University of Technology, Guangzhou 510641, China*

[b] *School of Civil Engineering and Transportation, South China University of Technology, Guangzhou 510641, China*

[c] *School of Marine Science and Engineering, South China University of Technology, Guangzhou, 511442, China*

[d] *PowerChina Renewable Energy Co., LTD., Beijing, 100101, China*

[e] *School of Water, Energy and Environment, Cranfield University, Cranfield MK43 0AL, United Kingdom*

Abstract

Floating Photovoltaic (FPV) systems are emerging as a new type of ocean renewable energy, offering advantages such as avoiding land use and promoting power generation efficiency. Providing significant cost-effectiveness for manufacturing, transportation, and installation, FPV systems with modular floating platforms exhibit the potential to replace the conventional large steel-frame one. However, the performance of such multi-floating body structures under wave conditions remain underexplored. In this paper, based on potential flow theory, the motion characteristics and power performance of the proposed FPV array connected by the articulated system are evaluated. The results indicate that the FPV arrays with shorter floating structures exhibit greater pitch motion, especially when the wave condition matches the pitch resonance. For multi-float cases, the articulated system, optimized with appropriate parameters, demonstrates efficacy as attenuators. Additionally, the proposed FPV array has great potential to serve as an infrastructure for integrating solar and wave energy. For a selected offshore site, potential wave energy output from motion attenuators between FPV floaters is assessed together with solar energy output. Overall, this study serves as a valuable reference for the design and optimization of the multi-modules FPV and advances the research on combined solar and wave energy utilization on floating structures.

Keyword: Marine Renewable Energy, Floating Photovoltaic, Ocean Engineering, Wave Energy Converters, Offshore Solar-Wave Combination

* Corresponding author

E-mail address: zhoubinzhen@scut.edu.cn (B. Zhou)

1. Introduction

Regarded as one of the most promising energy alternatives, the application of solar energy has experienced substantial growth in the renewable energy market over the past decades. The solar photovoltaic (PV) system is the typical approach for converting solar energy into electricity through the photogenerated current effect of PV cells. In recent years, the capacity of PV systems has been increasing significantly and is expected to reach 22% of global electricity in 2025 [1]. However, land requirement issues are the main barriers to the development of PV plants, as over 10,000 m^2 of land area is required for setting up a 1 MWp power station [2]. The floating photovoltaic (FPV) systems offer promising solutions to long-term energy demands, as they cover water bodies instead of valuable land resources for installation [3]. Besides, due to the water-cooling effect, FPV systems can achieve higher power generation efficiency [4]-[6]. In recent years, since many countries made significant efforts to develop FPV technology, researchers have started working in this area and engaged in addressing its practical challenges and outlining potential future trends of the FPV technology [7]-[9]. Structural safety and dynamic behaviour are the main concerns for the design of the FPV systems, especially for the offshore FPV due to insufficient technological maturity and exposure to severe environmental conditions, in which wave loads are predominant [10]-[12]. Ranjbaran et al. [13] summarized several main components of the FPV systems and indicated that the separate floats design and modular design are two of the most important factors that affect the performance of the FPV system. Dividing a long floating structure into several modules can significantly help reduce hydroelastic structural issues and ensure safety and long-term reliability in offshore ocean conditions [14]. Also, FPV systems with modular floating structures can offer significant cost-effective for manufacturing, transportation, and installation and there is a trend to adopt standardized lightweight floating modules connected by semi-rigid or flexible connectors in the FPV industry, instead of comparing to the integrated FPV structures [15]-[16]. As a result, it is also increasingly gaining scientific interest in recent years, and several effective studies have been carried out [17].

The connections between floating FPV modules are the critical components in modularized floating structures, greatly affecting the complex interaction of floaters hydrodynamics and have been widely investigated in recent years. Song et al. [18] investigated the dynamic response of the FPV system with vertical cylinders. The dynamic response of the floater connected with a fixed connector and hinged connector are compared under both normal operating and extreme wave conditions. Lee et al. [19] performed a comparison of experiment and numerical analysis of the FPV array with hinge connection and revealed that heave and pitch motions were dominant for head sea conditions. Jiang et al. [20] proposed soft connections

using elastic rope to avoid the large wave-induced bending moments transmitting between the floaters. The proposed multi-body FPV array exhibits excellent motion performances with the neighboring modules will not collide with each other under the extreme sea state. Song et al. [21] investigated the dynamic response of the FPV array using the articulated joint for flexible connection. Good seakeeping and stability were obtained, and they found that the resonance effect will be greatly affected by the relationship between the wavelength and the length. Overall, hinge connection is widely acknowledged as the suitable connection type for the FPV application since it can provide greater flexibility and resilience, allowing relative movement between adjacent modules induced by waves. Several studies on the motion behavior of hinge-connected floating bodies have been carried out [22]-[24].

However, for rigid connections, there may be a potential drawback in structural stiffness and stability [25], and therefore factors such as the module size, parameters of the articulated system and the platform geometric parameters should be taken into account to ensure the optimal design the modular FPV [26]. Tay et al. [27] emphasized the hydroelasticity of multi-connected modular offshore FPV and the results show that the FPV with a smaller aspect ratio have greater elastic deformation and the hydroelastic response could be reduced by increasing the longitudinal stiffness of the structures. Song et al. [28] investigated the characteristics of the multiconnected floating system and found that the tendency of the maximum response converged at 10 × 10 array while the installation direction and floater size can be further optimized to mitigate the dynamic and structural behaviors of FPVs. Wei et al. [29] evaluated the motion characteristics and expansibility of modularized floaters and concluded that the relationship between structure length and wavelength is a crucial parameter governing the motions of the FPV array. Zhu et al. [30] conducted a study on the hydrodynamic interactions of a co-located FPV array and offshore wind turbines, aiming to clarify the effects of solar platform geometric parameters on the hydrodynamic behavior of the hybrid system and indicate the potential for synergies between wind and solar energy. Previous studies have proved that the dimension of modules is the critical aspect that could significantly influence the applicability of the FPV array. A longish floating structure may experience large bending loads which may lead to structural failure while the smaller modules may require more connections and result in additional costs and larger motion response. The influence of module size on the FPV array under the interaction with ocean waves is critical but has rarely been discussed. As for the articulated system, the hinge connectors with appropriate damping and stiffness coefficients have a buffer effect, mitigating the interaction between floaters, while the connectors with high values of coefficients may fail to resist extreme environmental loads. Furthermore, inspired by the raft-type wave energy converters [31]-[32], the articulated system

can be regarded as the power take-off (PTO) system, comprising an integrated system [33]-[36] that can capture both solar energy and wave energy. The coefficients of articulated systems are worth investigating and optimizing but have rarely been investigated.

This study aims to fill the research gaps and its novelties are as follows: Firstly, the influence of the relationship between the wavelength and the length on the motion response and connector force under a wide range of wave conditions is investigated, providing reference for the deployment of the FPV. Second, the articulated system with appropriate coefficients acts as not only the attenuator but also the power take-off system of the wave energy; an offshore site is selected, with the motion response and combined solar and wave power generation performance evaluated under operation sea states.

The remainder of the paper is organized as follows. In Section 2, the constrained motions of the FPV array are mathematically modeled and validated by the well-proven code in Section 3. Section 4 presents the configuration of the multi-module FPV model and the performance criteria of the FPV system. In Section 5, the dynamic features, contact forces of the connectors, and the power performance of the FPV system are given. Also, an evaluation of the solar-wave hybrid system is done based on the selected operation sea states. Finally, Section 6 outlines the conclusions

2. Mathematical model

2.1 Hydrodynamics

The coupled hydrodynamic coefficients of the floats are calculated by the higher-order boundary element method (HOBEM) code WAFDUT [37]. Based on potential flow theory, the fluid is assumed to be incompressible, and inviscid, and the flow is irrotational. The velocity potential φ that satisfies the Laplace equation in the whole fluid, and the following boundary conditions on the free surface (z=0), the submerged part of floating body surface S_b and the seabed S_d is introduced:

$$\nabla^2\varphi = 0 \tag{1}$$

$$\left.\begin{aligned} \frac{\partial\varphi}{\partial z} - \frac{\omega^2}{g}\varphi = 0 \quad & z = 0 \\ \frac{\partial\varphi}{\partial n} = V \quad & \text{on } S_b \\ \frac{\partial\varphi}{\partial z} = 0 \quad & \text{on } S_d \end{aligned}\right\} \tag{2}$$

In linear potential flow theory, the total velocity potential can be decomposed into three parts, which are contributions from the incident wave potential φ_I, diffraction velocity potential φ_d

and radiation velocity potential φ_r, respectively.

Based on the linearized Bernoulli equation, the pressure distribution on the wet surface of the floating body can be obtained by the following equation:

$$\boldsymbol{f} = -\rho\iint_{S_b}\left[gz - \mathrm{i}\omega(\varphi_i + \varphi_d + \varphi_r)\right] - \rho g\iint_{S_b}\left[\boldsymbol{\xi} + \boldsymbol{\alpha}\cdot(\boldsymbol{x} - \boldsymbol{x}_0)\right]\cdot\boldsymbol{n}_3\boldsymbol{n}\mathrm{d}s \tag{3}$$

where g is the fluid density and the 2nd term of the equation refers to the restoring force generated since the floating bodies deviated from their equilibrium position.

2.2 Constrained dynamics

The constrained motion equation of the multi-floating-body system in the frequency domain can be expressed as[38]:

$$\begin{bmatrix} -\omega^2(\mathbf{M}+\mathbf{a}) + \mathrm{i}\omega(\mathbf{b}+\mathbf{b}_{\text{hinge}}+\mathbf{b}_{\text{vis}}) + \mathbf{k}_r + \mathbf{k}_m + \mathbf{k}_{\text{hinge}} & \mathbf{C}_{\mathbf{X}}^{\mathrm{T}} \\ -\omega^2\mathbf{C}_{\mathbf{X}} & \mathbf{0} \end{bmatrix}\begin{bmatrix} \boldsymbol{\xi} \\ \boldsymbol{f}_L \end{bmatrix} = \begin{bmatrix} \mathbf{F}_{ex} \\ \mathbf{0} \end{bmatrix} \tag{4}$$

where ω refers to the angular frequency of the incident wave. $\mathbf{a}=a_{ij}$ and $\mathbf{b}=b_{ij}$ ($i, j=1, 2\ldots6n$) are the $6n\times6n$ added mass matrix and radiation damping matrix, respectively, and n is the total number of the floating bodies. $\mathbf{b}_{\text{vis}}$ is the viscous damping matrix, $\mathbf{k}_r$ is the hydrostatic restoration matrix and $\mathbf{k}_m$ is the equivalent mooring stiffness matrix. The damping and stiffness coefficient of the hinge connectors are demoted as $\mathbf{b}_{\text{hinge}}$ and $\mathbf{k}_{\text{hinge}}$. $\boldsymbol{\xi}$ is the $1\times6n$ vector of the system motion response while the $\mathbf{F}_{ex}$ is the $6n\times1$ vector of the wave excitation force acting on the system. $\boldsymbol{f}_L$ refers to the forces and moments caused by the constraints between buoys and is the $5n\times1$ matrix. The constraint relations of the system can be expressed in matrix form[39]:

$$\mathbf{C}(\mathbf{X}) = \left[C_1(\mathbf{X})\ \ C_2(\mathbf{X})\ \ C_3(\mathbf{X})\ \ C_4(\mathbf{X})\ \ C_5(\mathbf{X})\right]^{\mathrm{T}} = \mathbf{0} \tag{5}$$

where $C_i(\mathbf{X})$ corresponds to the constraints in the five DoFs except for pitch. $C_i(\mathbf{X})$ is the $5\times6n$ linear constraint Jacobian matrix of $\mathbf{C}(\mathbf{X})$. The form of $\mathbf{C}(\mathbf{X})$ and $C_i(\mathbf{X})$ can be formulated through multi-body dynamics. More details of the constraints matrix can be found in Ref [40].

The multi-structure time-domain constrained dynamic equation can be derived from Cummins' formulation[41]:

$$\begin{bmatrix} \boldsymbol{M}+\mathbf{a}(\infty) & \boldsymbol{C}_{\mathbf{X}}{}^{T} \\ \boldsymbol{C}_{\mathbf{X}} & 0 \end{bmatrix}\begin{bmatrix} \ddot{\boldsymbol{\xi}}(t) \\ \boldsymbol{f}_L \end{bmatrix} = \begin{bmatrix} -\int_{-\infty}^{t}\boldsymbol{\kappa}(t-\tau)\dot{\mathbf{X}}(t)d\tau - \mathbf{k}_r\mathbf{X}(t) + \boldsymbol{F}^{\text{Wave}}(t) + \boldsymbol{F}^{\text{Moor}}(t) + \boldsymbol{F}^{\text{vis}}(t) + \boldsymbol{F}^{\text{hinge}}(t) \\ 0 \end{bmatrix} \tag{6}$$

where $\mathbf{a}(\infty)$ represents the matrix of added mass for infinite wave frequency. $\boldsymbol{\kappa}(t-\tau)$ is the matrix of radiation impulse response function, which can be determined through a refined Filon quadrature method proposed by Liu [42]. More details of the time-domain constraint equation could be referred to Ref [43].

3. Validation

To validate the accuracy of the established multiple structures hydrodynamic interaction numerical model, the modeling is compared with the simulation results proposed by Chen *et al.* [44]. The configurations of the validation model consisting of three rectangular floaters are shown in Figure 1 and some of the parameters are summarized in Table 1. In this study, the pitch motion of multi-float, which will greatly affect the sunlight absorption efficiency of FPV, under wide ranges of wave frequencies is the main focus. Thus, in Figure 2, the result of pitch and heave response amplitude operators (RAOs) of each float, with the wave frequency ranging from 0.01 rad/s to 2.41 rad/s is compared to the well-proven code given in Ref [44]. A good agreement is achieved with a maximum error of less than 4%, illustrating that the developed model is capable of simulating the hydrodynamic interaction of multiple structures under waves.

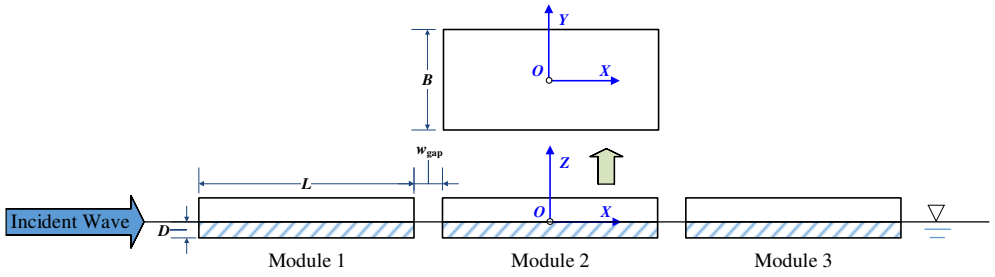

Figure 1 Plan view of the validation model[44]

Table 1 The properties of the single floating module[44]

Module Characteristic	Value
Length, L (m)	100
Breadth, B (m)	50
Draught, D (m)	2
Gap Width, w_{gap} (m)	5
Center of gravity above base, KG (m)	2.5
Radius of roll gyration, R_{xx} (m)	14.5
Radius of pitch gyration, R_{yy} (m)	28.9
Water Depth (m)	5

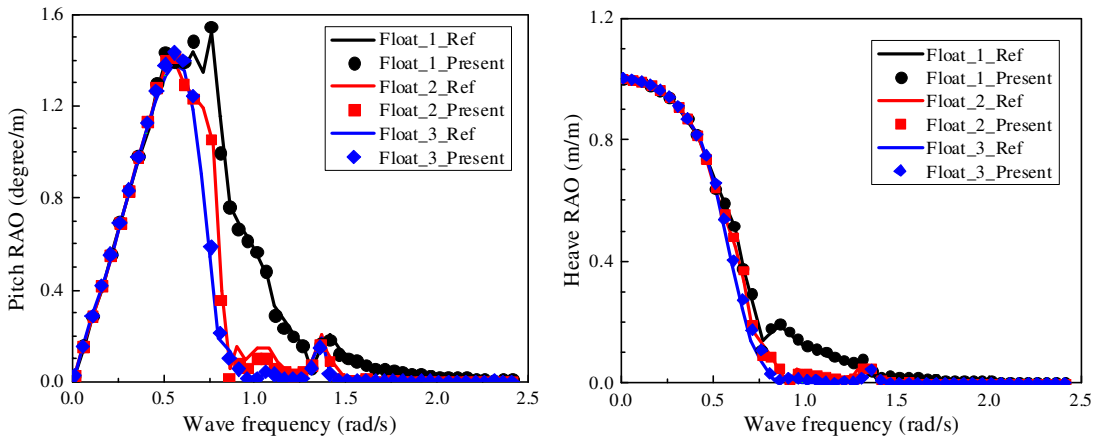

Figure 2 Comparison between the proposed numerical model and well-proven code

4. Set up of multi-module FPV model

In this study, the direction of waves is always parallel to the FPV array as shown in Figure 3. The existing studies [45] have already proved that the FPV array suffered the maximum wave loads in this case and the transverse wave force within the FPV array is significantly smaller than that in the longitudinal direction, which means the dynamic response of each row of the FPV system is similar. Therefore, the FPV array can be simplified to a single row of FPV located in the middle part of the array, as shown in Figure 3. A longish floating structure may experience large bending loads while a shorter one may require more connections and lead to additional construction costs. To investigate the dynamic performance of different dimensions of floating structures, a large single-row of FPV structure is divided into 2, 3, 4, 5 and 6 parts respectively and connected by hinge connectors with a 1 m gap between adjacent bodies, and the hinge connectors are numbered sequentially along the positive x-axis, as shown in Figure 4. The length of the total floating structure L_T is fixed at 49 m. In addition to their connecting function, these hinge connectors, equipped with damping and stiffness coefficients, serve multiple roles, acting both as motion attenuators and raft-type wave energy converters. The dimensions and viscous damping (obtained from free-decay tests using CFD Software Star CCM+) of the individual floater of each case are listed in Table 2. The hinge connectors can constrain two structures and only allow them to rotate around a single axis. The equivalent mooring stiffness matrix calculated by the open-source mooring analysis program [46] is given in Table 3.

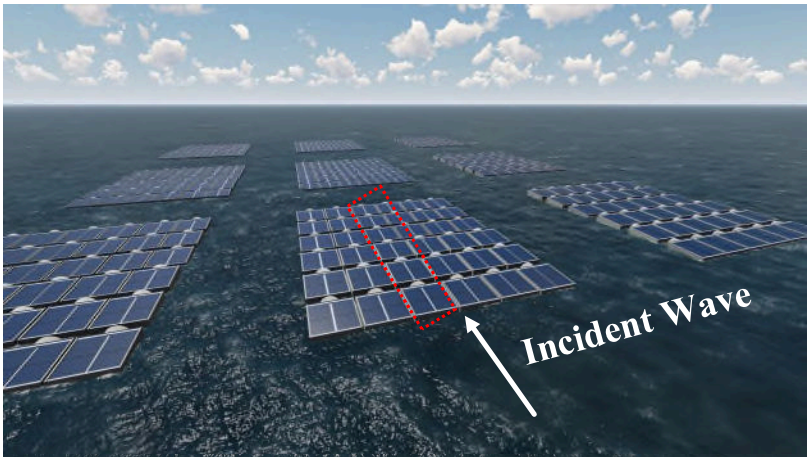

Figure 3 Sketch of the large floating solar farm

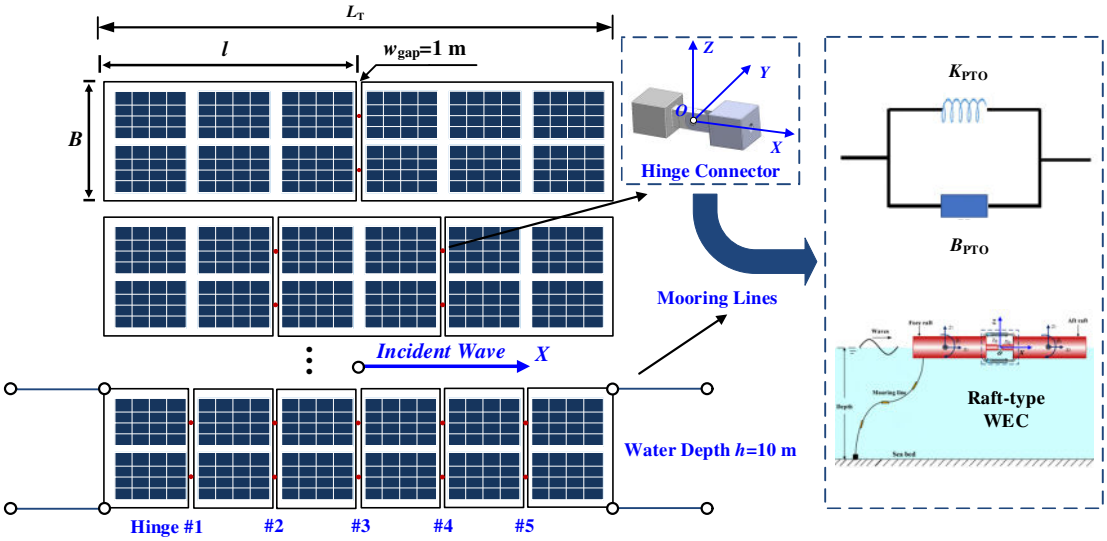

Figure 4 Configuration of the single-row of FPV

Table 2 Key parameters of different layouts of FPV

Case	Number of Floats	l (m)	B (m)	D (m)	b_{vis} (kN*m/rad)
A	2	26	6	1	3.61E+03
B	3	17	6	1	1.09E+03
C	4	12.5	6	1	3.79E+02
D	5	9.8	6	1	1.66E+02
E	6	8	6	1	7.03E+01

Table 3 Equivalent mooring stiffness matrix

4.53E+03	0	0	0	0	0
0	1.26E+05	0	-2.07E+05	0	0
0	0	4.38E+04	0	0	0
0	-2.07E+05	0	6.25E+05	0	0
1.43E+00	0	0	0	3.08E+07	0
0	0	0	0	0	8.92E+07

Several parameters which are defined and used to evaluate the hydrodynamic performance of the single-row FPV investigated in this paper, are shown in Figure 5. As for motion response, more attentions are paid to the pitch motion since the solar irradiance on the tilted plane can be obtained by [47]:

$$E(\mathrm{t}) = B_{\mathrm{h}} \cos\theta_{\beta} + D_{\mathrm{h}} \cos^{2} \frac{(1+\cos\beta)}{2} + G_{\mathrm{h}} \frac{(1-\cos\beta)}{2} \tag{7}$$

where B_{h}, D_{h} and G_{h} are the direct beam, diffuse, and reflected radiation irradiances on the horizontal plane, respectively. θ_{β} is the incidence angle of solar radiation on the tilted plane and β denotes the tilt angle of the plane, and both are determined by the pitch angle of the floating bodies.

Pitch amplitude shows the largest pitch motion of each floater in the frequency domain under wide ranges of regular waves. The solar radiation absorption can be roughly equivalent to the effective length of the FPV array under working conditions which can be calculated by:

$$L_{\mathrm{E}} = \sum_{i}^{n} L_i \cdot \cos\theta_i \tag{8}$$

where L_i and θ_i are the structure length and the average pitch angle of the i floating body, respectively. n is the total number of floating bodies.

The contact force that hinge connectors suffer can be divided into F_{conX} and F_{conY}. With damping and stiffness constraints taken into account, hinge moments around the Y-axis should be considered.

The damping coefficients of the articulated system can be assumed to be the linear power take-off damping b_{PTO}. The PTO control torque of the linear damping can be expressed as:

$$\tau_{\mathrm{PTO}} = b_{\mathrm{PTO}} \Delta\dot{\theta}(t) \tag{9}$$

where $\Delta\theta$ and $\Delta\dot{\theta}$ are the angular displacement and velocity of two adjacent floating bodies connected by a hinge connector. Assuming the stiffness coefficient is zero (k_{PTO}=0), the PTO system will only attenuate the response without moving the resonance frequency of the structure. The PTO power can be obtained as follows[48]:

$$P = \tau_{\mathrm{PTO}} b_{\mathrm{PTO}} \Delta\dot{\theta}(t) = b_{\mathrm{PTO}} \Delta\dot{\theta}^{2}(t) \tag{10}$$

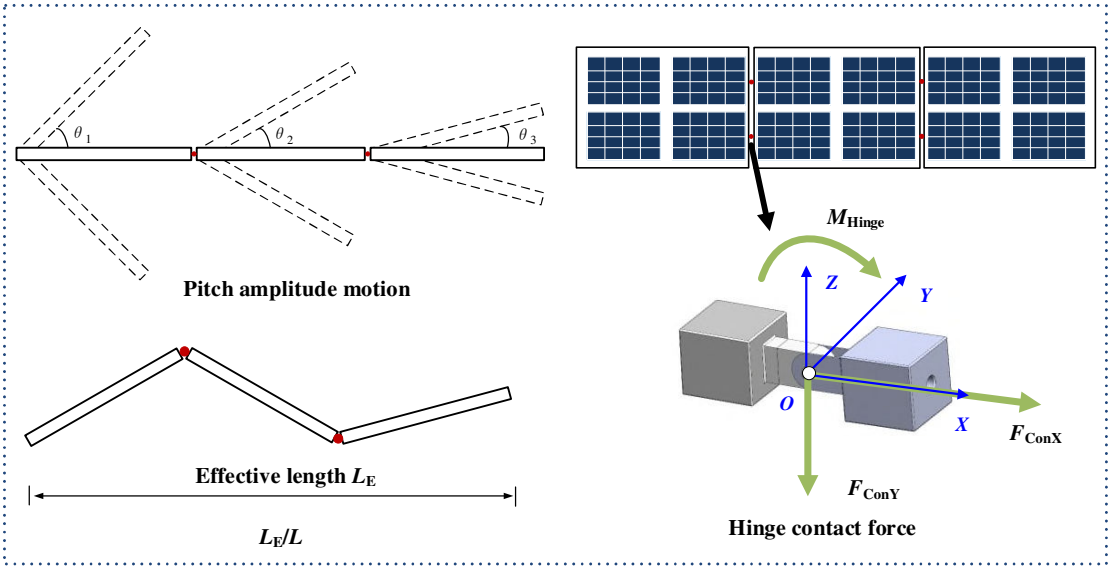

Figure 5 Parameters used to evaluate the performance of FPV

5. Results and discussion

5.1 Motion response

In this section, regular waves travel in the positive x-direction with a unit amplitude A and the dimensionless factor α (kl) ranges from 0.5 to 5.0. Dimensionless factor $\alpha=kl$, where k is the wave number and l is the length of the floating structure, is proposed to represent the relationship between the ratio of structure length to wavelength. The water depth h is 10 m. Figure 6 shows the pitch motion response, which may greatly affect the solar radiation absorption performance, of different dimensions of a row of FPV array. As the dimensionless factor α increases, the pitch motions of all floats show a trend of first increasing and then decreasing, reaching a peak when kl is around 2 to 3, which can be regarded as the pitch motion resonance frequency of each float. Larger pitch motion can be observed on the smaller modules since more hinge connectors and less structure mass allow them to move along with the waves and can be even visualized as flexible thin film when a sufficient number of connectors are assembled. In most cases, the highest motion occurs at the first float facing the wave directly, except for the Case E when kl is around 2.4 which may be affected by the relatively large added mooring stiffness compared to the wave exciting force acting on the float, resulting in larger pitch motion occurring at the rear floaters of the array in this case. Then, the motion response of the rest floating structures gradually attenuates along the wave-propagating direction since the motions of the front floaters dissipate the wave energy. The pitch motion of float No. 1 of each dimension is compared to that of Case A in Figure 7. The results show that only when the wavelength is too long or too short, the pitch motion of each structure dimension is almost the same with a relatively low level. In other cases, the pitch motion grows as the number of the

divided float increases, especially when *kl* is around 2.5.

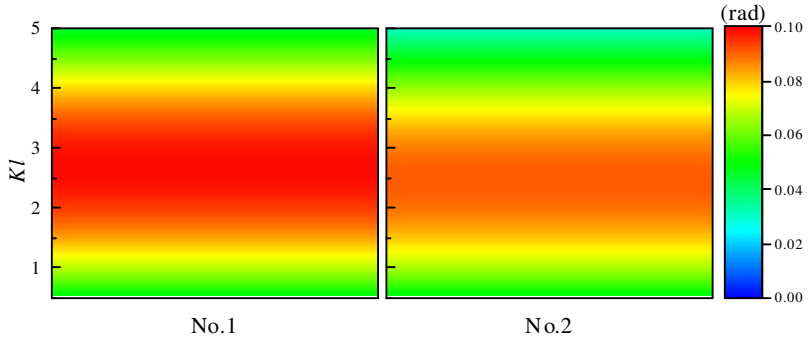

(a) Case A

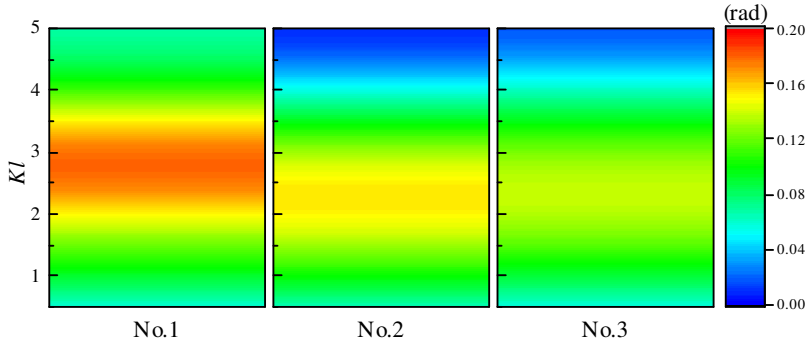

(b) Case B

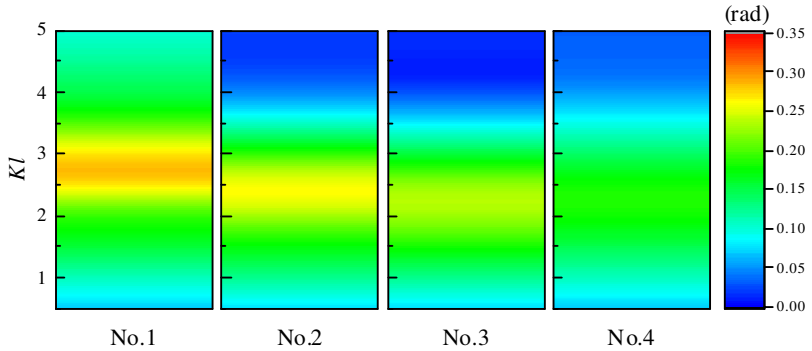

(c) Case C

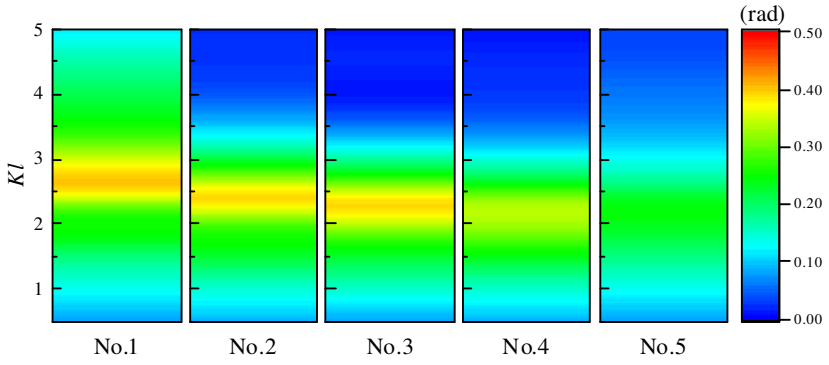

(d) Case D

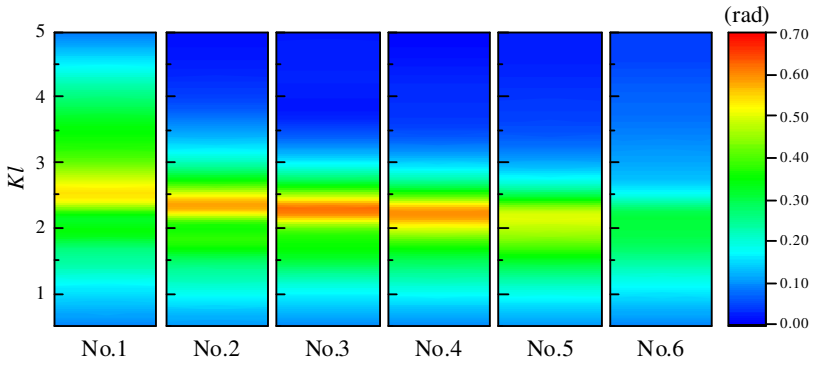

(e) Case E

Figure 6 Pitch motion response of different numbers of floats

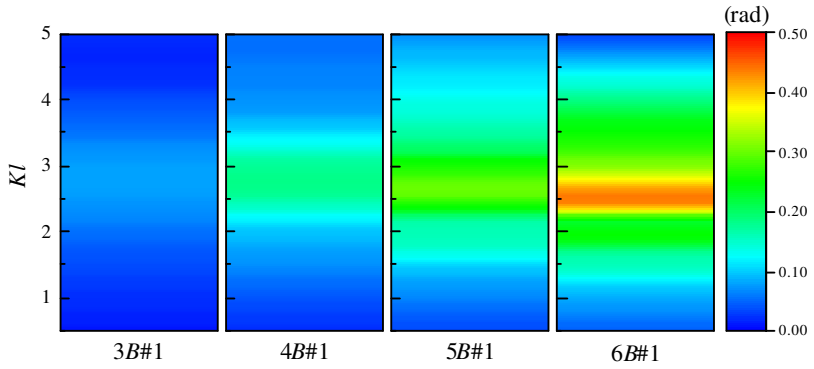

Figure 7 Pitch motion of float No. 1 of each dimension compared to that of two floats

The maximum pitch motion of the first float of different dimensions of structures and their corresponding wave periods are given in Figure 8. As the floating body number increases, the pitch amplitude increases while the corresponding wave periods decrease since the square root of the hydrostatic restoration to total inertia ratio grows as the dimension of the floating body decreases. The dimensionless factor α fluctuates around 2.5 as the number of floating bodies increases, showing the relationship between the ratio of structure length to wavelength and the pitch resonance. To achieve better motion response performance, the structure length should be well designed considering the wave conditions around the operation area to avoid resonance.

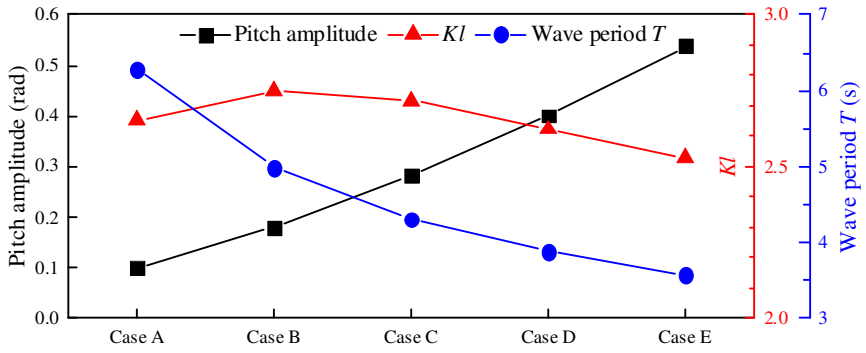

Figure 8 The maximum pitch motion of different dimensions of float No. 1 and their corresponding wave periods

5.2 Contact forces of hinge connectors

The hinge connectors should be regarded as the stress concentration areas, and the analysis of contact forces under wide ranges of waves is essential for the design of the connectors. The contact forces of each connector of different numbers of floats are given in Figure 9 and some statistical values are summarized in Table 4. Since the forces on the connectors are mainly affected by the multiple structures hydrodynamic force and motion response of the floating structures. Therefore, the first hinge connector connects the first float, which faces the incident wave directly and gets a larger motion response, with its adjacent float suffering a larger contact force in most cases. As for the hinge connector No.1 of different numbers of floats, the first and the only connector for Case A suffers the largest contact force, while the value decreases significantly as the float number is added to three. As the number of floating bodies keeps increasing, the force has not obviously eased except for the cases when the wavelength is too long or too short and the maximum of the contact force will increase. Comparing Figure 6 and Figure 9, when the number of floats is larger than three, the force of hinge connector No.1 shows consistent patterns with the pitch motion of float No. 1 and also obtains its peak value around the pitch motion resonance frequency. The results indicate that though the degrees of freedom that are constrained (Surge and Heave) have a greater impact on the force of the hinge connector, the pitch motion response of the floating structures contributes more to the force of hinge connector No.1 than motion in other DoF, around the resonant frequency. As for the rest of the connectors, the contact forces show different trends compared to hinge connector No.1, especially for Case C, Case D and Case E. The pitch motion response still plays an important role, since a sudden increase or decrease can be observed near the pitch motion resonance frequency.

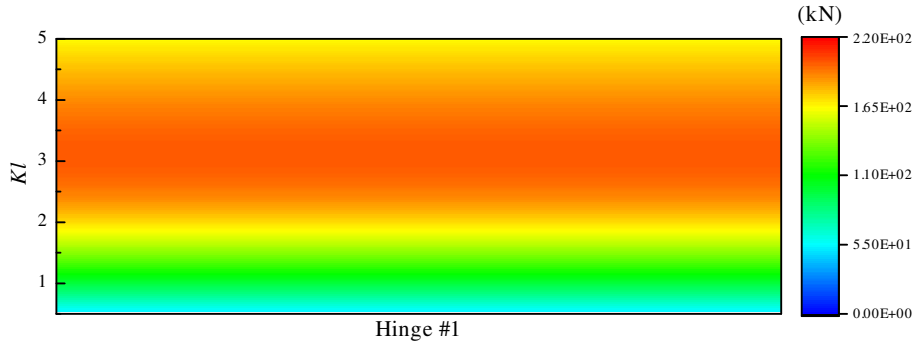

(a) Case A

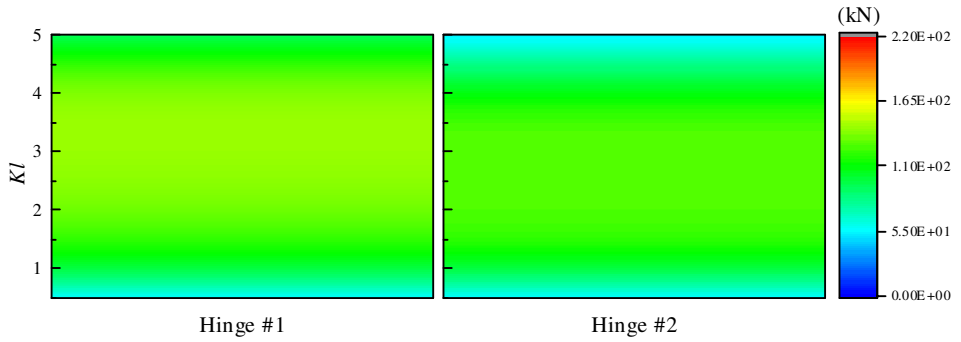

(b) Case B

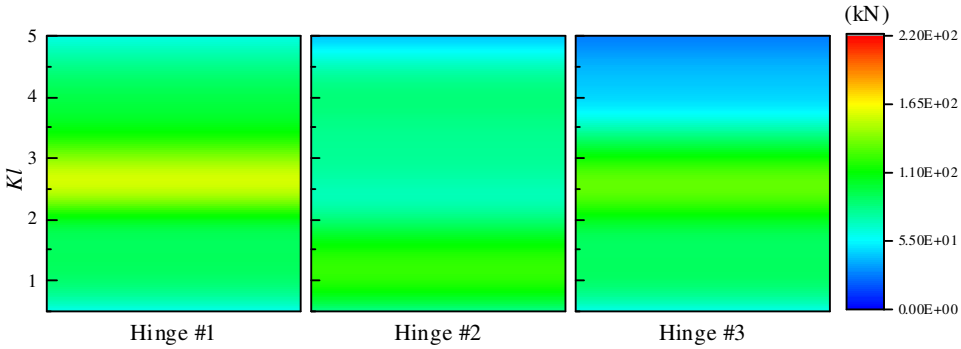

(c) Case C

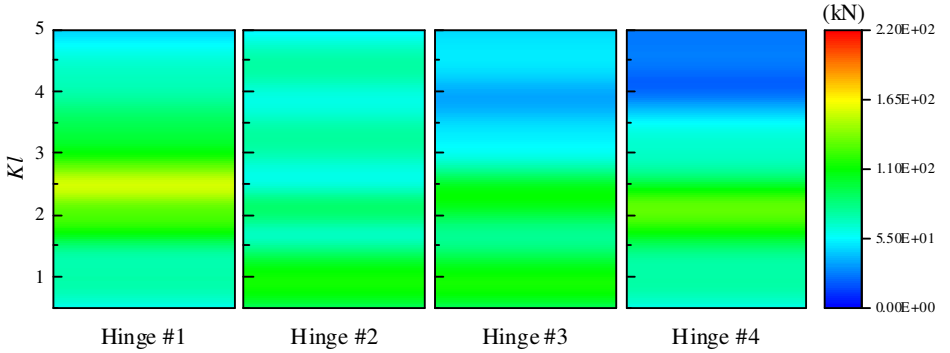

(d) Case D

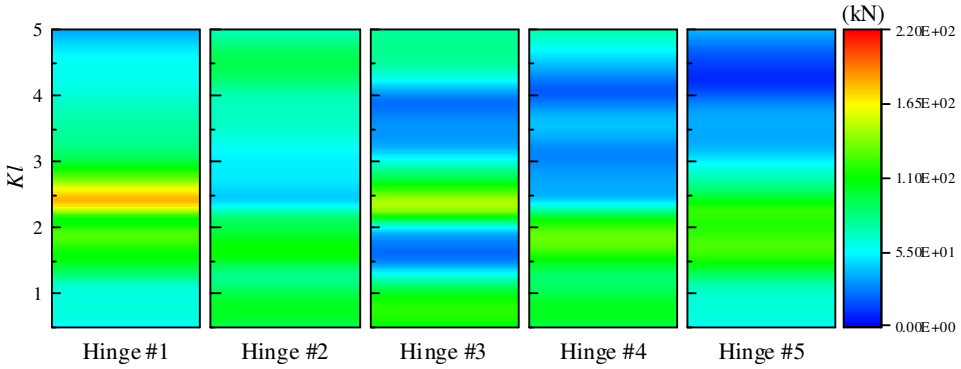

(e) Case E

Figure 9 The hinge connectors forces of different numbers of floats

Table 4 Statistical value of hinge connectors forces

Case	Connected Force		
	Max		Corresponding wave period (s)
	Value (kN)	F_{con}/F_{ex}	
A	200.48	0.35	5.81
B	143.38	0.48	4.55
C	155.95	0.55	4.36
D	155.60	0.68	4.00
E	180.11	0.95	3.65

The contact force is divided into four levels according to the magnitude, and the proportion of each part is given in Figure 10. Since the wave energy is dissipated by the front floaters, there is less possibility for the rest of the connectors to endure a larger constraint force. Multi-module designs could help alleviate the stress of the connectors while there is a limit for the number of floaters since the smaller structures will experience larger pitch motion, which also significantly contributes to the contact forces of hinge connectors.

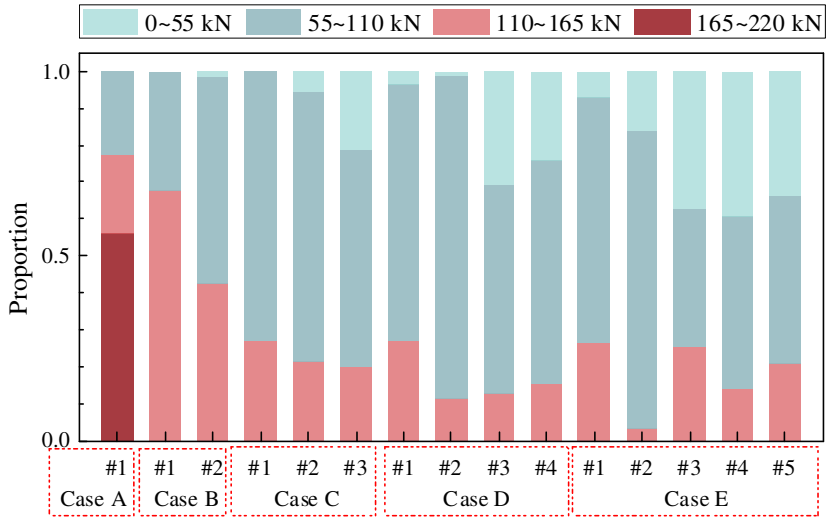

Figure 10 The proportion of different magnitudes of the hinge connectors forces

5.3 Influence of the coefficient of the articulated system

In Section 5.1, the results show that the pitch motion of floats will increase significantly under the specific wave frequency, especially for the multi-float cases. Large pitch motion may greatly affect the stability and energy absorption performance of the FPV system. The articulated system with proper damping or stiffness coefficients acts as the attenuator and is beneficial in suppressing the motion response. Figure 11 shows the trend of the ratio of effective length to structure length of different dimensions of a row of FPV array, with different damping or stiffness coefficients under the worse wave frequency. The corresponding dimensionless factor α fluctuates from 2.02 to 2.76 since the pitch motion resonance frequency for each float

in a row is slightly different as shown in Figure 7. For Case A and Case B, since the pitch motion for floats are quite low and the ratio L_E/L approximated to 1. Therefore, the added damping or stiffness coefficients seem to show no significantly positive effect in Case A and Case B. As the number of floaters increased, a larger pitch motion appears, and thus a marked decline of the ratio L_E/L can be observed with the value dropping to only 0.9325 in Case E.

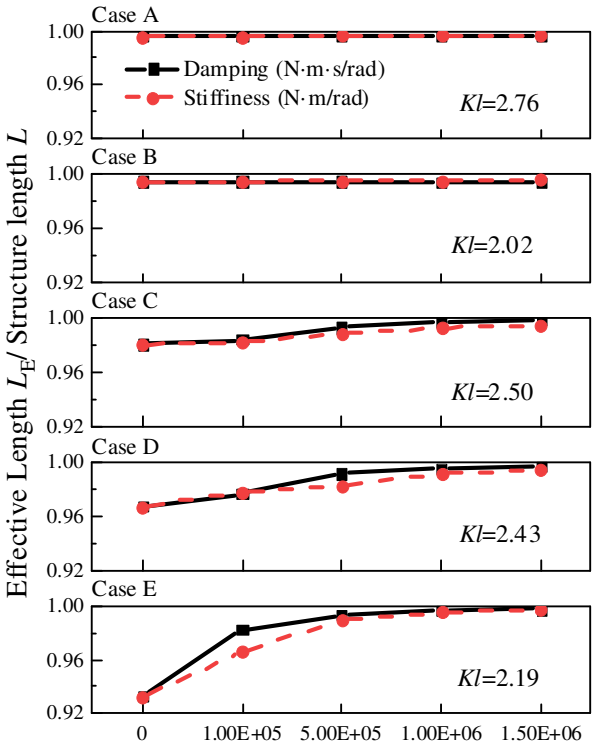

Figure 11 The effect of damping or stiffness coefficients contribute to effective length under the specific wave frequency

In Cases C-E, attenuators with damping or stiffness coefficients can significantly enhance the motion performance as illustrated in Figure 11. The average pitch motion of each float for Case C, D and E, with different damping or stiffness coefficients under the specific wave frequency are visualized in Figure 12. The pitch motion of each float diminishes as the damping or stiffness coefficient increases and ultimately reaching a stabilized state with the ratio L_E/L is approximated to 1. The performance of the damping coefficient on inhibiting large motion response is slightly better than that of the stiffness coefficient. In Figure 12, larger motions can be observed on the first float of the array in Case C, and D while they appear on the three or four floats in Case E since affected by the relatively large mooring stiffness. Taking the cost of the articulated system into account, deployed damping or stiffness mechanism only in the specific hinge connector which connected the floats with the largest pitch motion can also work pretty well for motion attenuation. Comparisons of the ratio L_E/L of different arrangements of the damping mechanism are given in Figure 13 and the damping coefficient is set as

b=1.50E+06 N*m*s/rad. Significant improvement in effective length can be obtained with the damping mechanism only added to one hinge connector with the ratio L_E/L almost approximated to 1 in Case C and Case D and there is no obvious benefit with more damping mechanism added. As for Case E, though adding the damping mechanism into hinge#3 can also obviously increase the ratio L_E/L, with a growth rate of 5.68%, the motion performance can be further improved with more damping mechanisms added, since there are several floats with large pitch motion in this case. The articulated system of FPVs is in a similar structure to the flap-type wave energy converter, which means with the power take-off (PTO) system integrated, the articulated system can capture wave energy as well as suppress the pitch motion. The proposed FPV array has great potential to serve as an infrastructure for combining solar energy and wave energy.

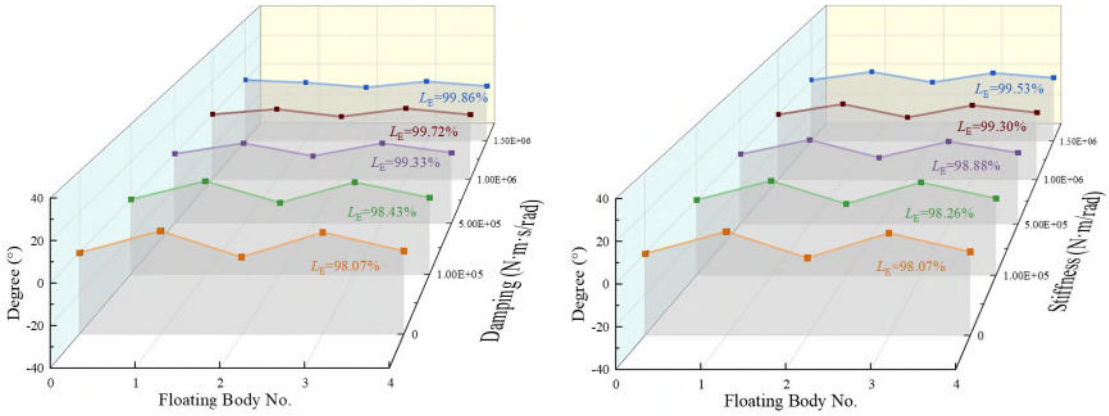

(a) Case C

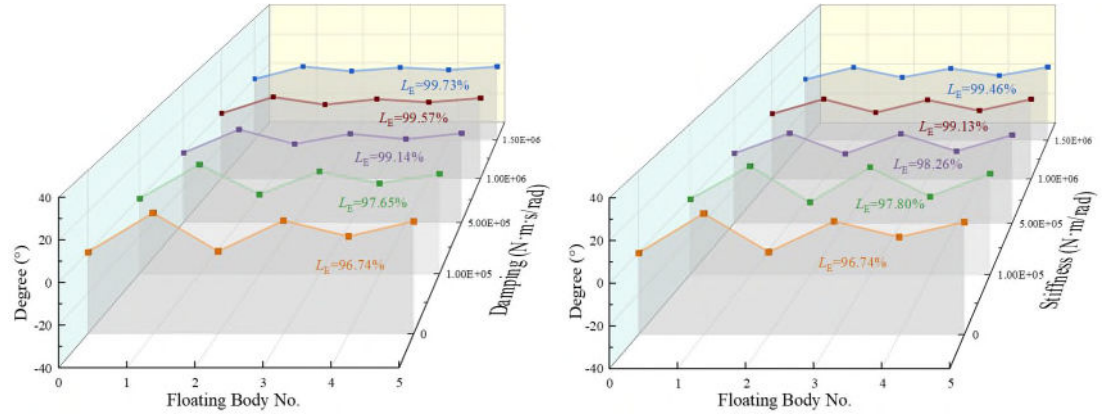

(b) Case D

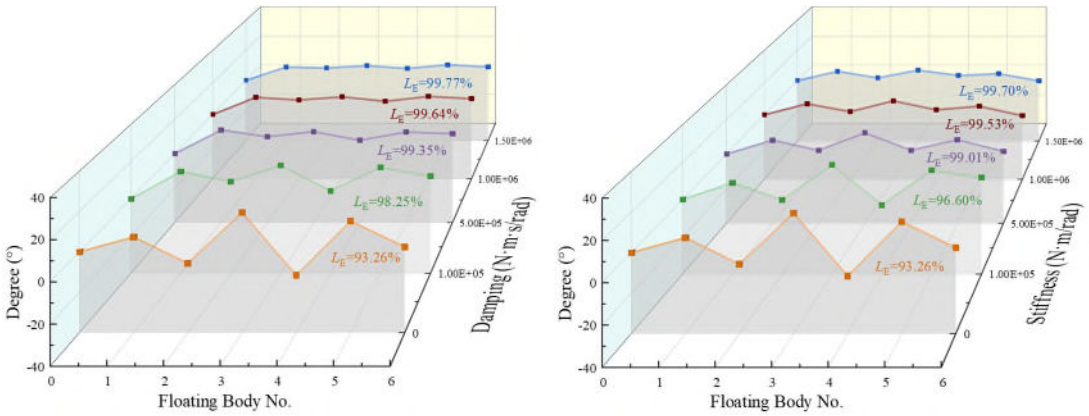

(c) Case E

Figure 12 The average pitch motion of each float with different damping or stiffness coefficients under the specific wave frequency

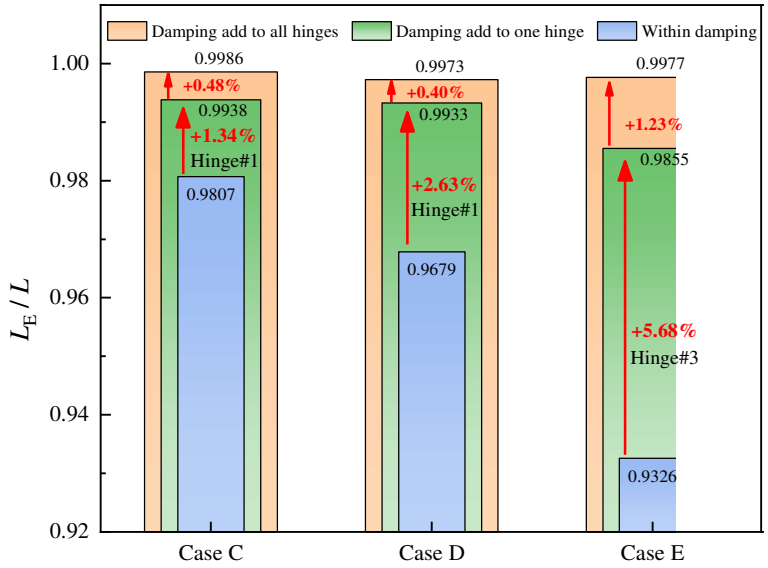

Figure 13 Comparison of different arrangements of the damping coefficient in the articulated system

5.4 Solar and Wave Energy performance for the selected operation site

The selected operational site of the FPV system is located in the northern part of the South China Sea and the wave environments were obtained in a field study (114°58′E, 21°16′N)[49]. The peak of the FPV array under the regular wave (T=5.3 s), including the ratio L_E/L, the maximum constraint force and the maximum articulated system torque, is shown in Figure 14. Since the wave frequency around the selected operational site is distanced from the resonance frequency of the floating structures, the effective length of the FPV can remain at a relatively high level though it decreases slightly as the floating structure is divided into more parts. With the damping or stiffness coefficients added to the articulated system, the effective length L_E of all the cases gradually grows and the ratio L_E/L of all the cases almost comes up to the same level as the damping coefficient reaches b=1.50E+06 N*m*s/rad or stiffness coefficient reaches

k=1.50E+06 N*m/rad. The addition of the damping or stiffness coefficients has no obvious impact on the maximum constraint force and the maximum constraint force always shows a downward trend as the number of floating bodies increases. Compared to Case A, the maximum constraint force of the hinge connector has dropped by nearly 59.17%. The torque of the articulated system resulting from the damping or stiffness coefficient should be also taken into account since it can be regarded as the PTO force of the wave energy converters and will greatly affect the wave energy absorption performance of the wave-solar hybrid system mentioned in Section 5.3.

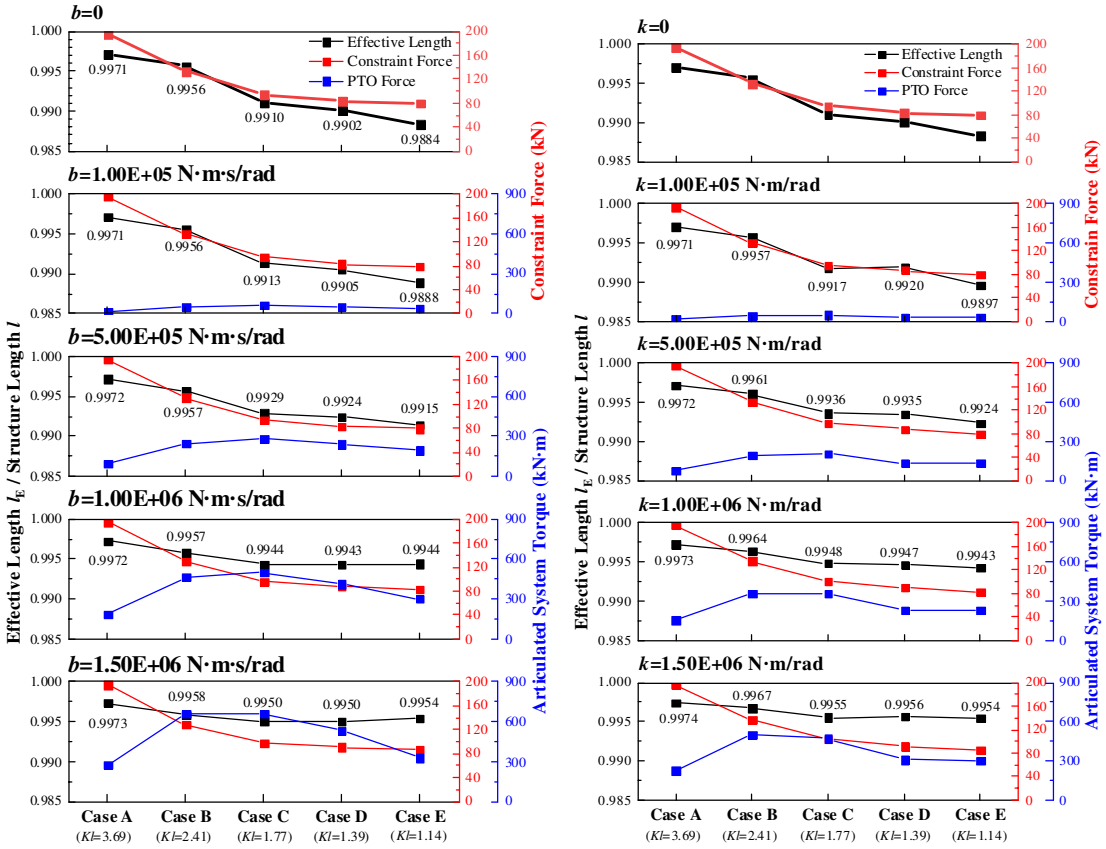

(a) Damping coefficient (b) Stiffness coefficient

Figure 14 Performance of different arrangements of the FPV array under wave period T=5.3 s

The power performance of the FPV array with the damping coefficient of the articulated system setting as b=1.50E+06 N*m*s/rad under irregular waves according to the selected environmental condition is evaluated and the JONSWAP spectrum is used. The solar radiation on the floating planes tilted at 30° at noon on the day of the winter solstice is calculated, and the time histories of the unit solar radiation of different cases are given in Figure 15 and the key statistical parameters are summarized in Figure 16. The results show that though the solar radiation fluctuates compared to the fixed plane, resulting from the pitch motion, the average value is very close to that of the fixed plane, within the maximum difference of 0.07%, with a

relatively low standard deviation. This stability is achieved with the aid of a large damping coefficient (b=1.50E+06 N*m*s/rad) in the articulated system, which has proven to be significantly effective in inhibiting motion response. The solar radiation absorption performance of different cases is consistent with the results of effective length shown in Figure 14 a, which can prove that the results calculated in the frequency domain can be applied for preliminary evaluation of FPV absorption performance and it is a good method for quick optimization while saving computing resources.

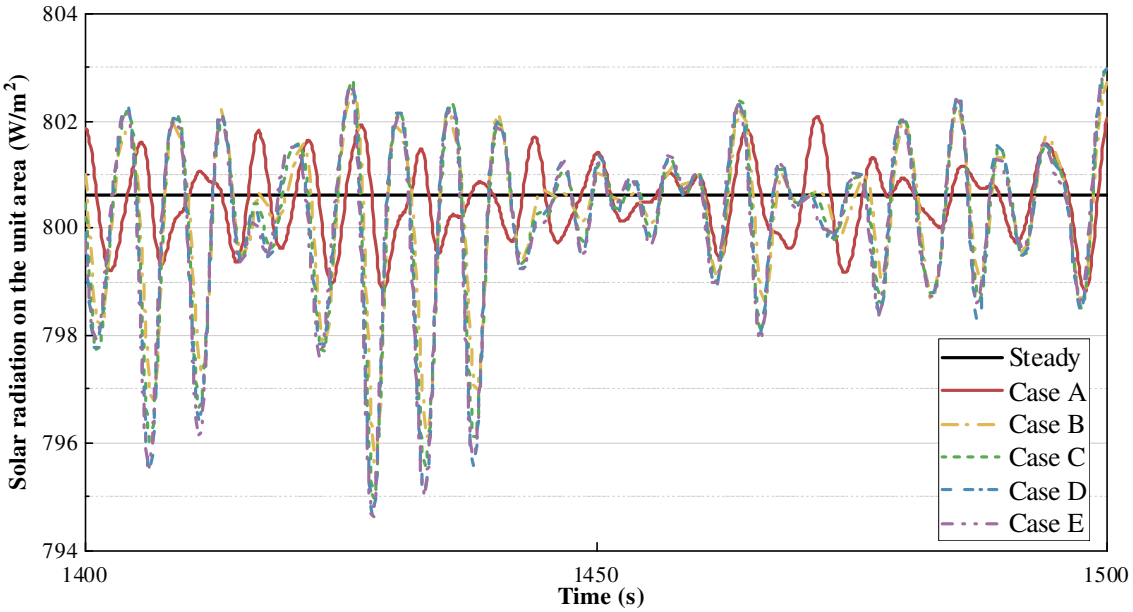

Figure 15 Unit solar radiation time histories of different cases under the wave environments of the selected operational site

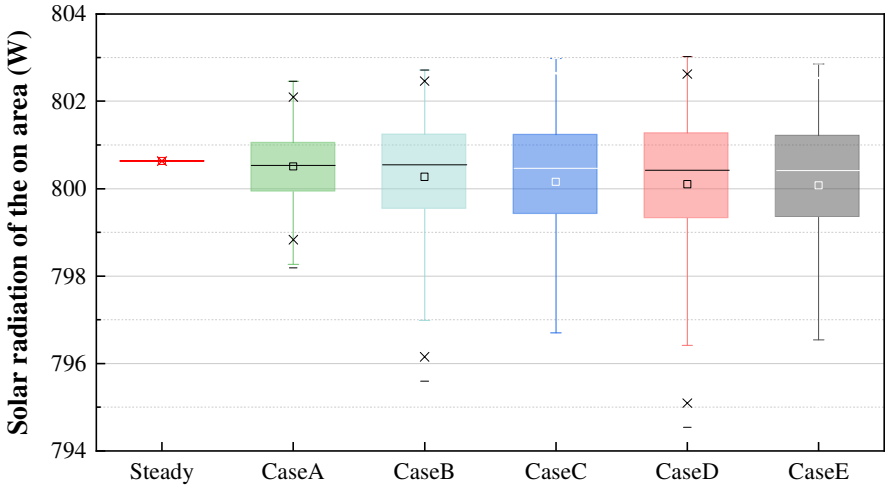

Figure 16 Box-plot of the unit solar radiation

The damping mechanism in the articulated system can be assumed as the linear power take-off (PTO) system of wave energy. The efficiency of PV systems is limited to 20%[50]. The average power generation of the wave-solar hybrid system is given in Figure 17. With more

hinge connectors added, the total average solar energy generation slightly decreases, with a maximum decrease of 7.74%, resulting from the less effective area. On the contrary, the wave energy contributes more to the total energy output as the number of floating bodies increases, peaking at 36.32% in Case D, and then the value declines since the PTO forces drop significantly as shown in Figure 14 a. In all these cases, the wave power generated by the 1# hinge connector is considerably greater than others and the power generation of the rest of the hinge connectors gradually decreases since the wave power is attenuated. It can be concluded that the proposed wave energy converter provides considerable power compared to the FPV system. Also, wave power, which is accessible about 90% of the time, could be an effective supplement while solar energy is experiencing downtime. Furthermore, in this study, the PTO damping coefficient is set for attenuating the pitch motion for the floaters and it is not the optimal PTO damping for wave energy capturing. Overall consideration of PTO damping and spring–stiffness coefficient for both motion response and power generation of the hybrid system should be taken in future works.

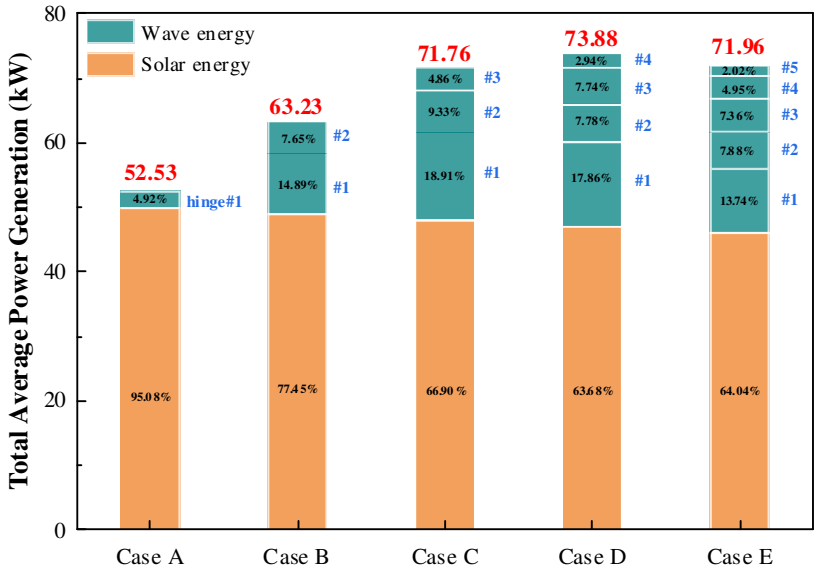

Figure 17 The power generation of the hybrid system under selected operational site

6. Conclusions

A multi-module offshore floating photovoltaics system, interconnected by an articulated system is proposed and the influence of module dimensions and hinge connectors coefficient on the motion response and power generation performance of the FPV array is investigated. The numerical model based on the potential flow theory and multi-body dynamics is established and verified by the presented well-proven codes. The dynamic and power generation performance of the proposed FPV array is examined under a wide range of regular wave conditions and irregular wave conditions of the selected operation site. The main findings are

summarized as follows:

1. Larger pitch motion can be observed on the FPV array with shorter floating structures, particularly when the wave conditions coincide with the pitch resonance frequencies. To enhance motion response performance, proper design of the FPV array's structural length is essential to mitigate motion resonance. Since the wave energy is dissipated by the front floaters, the motion response of the rest floating structures gradually attenuates along the wave-propagating direction and more attention should be paid to the floaters on the front of the array.

2. The first hinge connector, connecting the floaters exhibiting significant pitch motion responses, suffers a larger contact force in most cases. The force on the connectors is mainly affected by the multiple structures' motion response. As the number of floats is greater than three, the pitch motion response contributes more to the contact force of connectors and the force of hinge connector No.1 obtains its peak value near the pitch motion resonance frequency.

3. Optimized articulated systems, incorporating suitable damping or stiffness coefficients, function effectively as attenuators and are beneficial to suppressing the motion response, especially for multi-float cases. Significant improvements in effective length can be achieved by incorporating a damping mechanism into just one specific hinge connector, which connects two buoys with the greatest motion, while further additions of damping mechanisms yield negligible benefits.

4. With the appropriate damping or stiffness coefficients added to the articulated system, the effective length, which represents the performance of solar radiation absorption, can remain at a relatively high level though it decreases slightly as the floating structure is divided into more parts. Furthermore, the proposed FPV array holds great potential as an infrastructure for synergistic utilization of solar and wave energy. The wave energy contributes more to the total energy output as the number of floating bodies increases, peaking at 36.32% in Case D. Wave power serves as an effective supplement during solar energy downtime.

Acknowledgement

This work is supported by the National Natural Science Foundation of China National Outstanding Youth Science Fund Project (52222109), the National Natural Science Foundation of China (52071096 and 52201322), Project of State Key Laboratory of Subtropical Building and Urban Science (2023ZB14), Guangdong Basic and Applied Basic Research Foundation (2022B1515020036 and 2023A1515012144).

Reference

[1] Ghosh A. A comprehensive review of water based PV: Flotavoltaics, under water, offshore & canal top[J]. Ocean Engineering, 2023, 281: 115044.

[2] Vyas M, Chowdhury S, Verma A, et al. Solar Photovoltaic Tree: Urban PV power plants to increase power to land occupancy ratio[J]. Renewable Energy, 2022, 190: 283-293.
[3] Cazzaniga R, Rosa-Clot M. The booming of floating PV[J]. Solar Energy, 2021, 219: 3-10.
[4] Refaai M R A, Dhanesh L, Ganthia B P, et al. Design and implementation of a floating PV model to analyse the power generation[J]. International Journal of Photoenergy, 2022, 2022.
[5] Kjeldstad T, Lindholm D, Marstein E, et al. Cooling of floating photovoltaics and the importance of water temperature[J]. Solar Energy, 2021, 218: 544-551.
[6] Peng L, Liu B, Zheng S, et al. A new dynamic 2D fusion model and output characteristic analysis of floating photovoltaic modules considering motion and environmental factors[J]. Energy Conversion and Management, 2023, 294: 117588.
[7] Shi W, Yan C, Ren Z, et al. Review on the development of marine floating photovoltaic systems[J]. Ocean Engineering, 2023, 286: 115560.
[8] Ghosh A. A comprehensive review of water based PV: Flotavoltaics, under water, offshore & canal top[J]. Ocean Engineering, 2023, 281: 115044.
[9] Claus R, López M. Key issues in the design of floating photovoltaic structures for the marine environment[J]. Renewable and Sustainable Energy Reviews, 2022, 164: 112502.
[10] Oliveira-Pinto S, Stokkermans J. Marine floating solar plants: An overview of potential, challenges and feasibility[C]//Proceedings of the Institution of Civil Engineers-Maritime Engineering. Thomas Telford Ltd, 2020, 173(4): 120-135.
[11] Ikhennicheu M, Danglade B, Pascal R, et al. Analytical method for loads determination on floating solar farms in three typical environments[J]. Solar Energy, 2021, 219: 34-41.
[12] Kumar M, Niyaz H M, Gupta R. Challenges and opportunities towards the development of floating photovoltaic systems[J]. Solar Energy Materials and Solar Cells, 2021, 233: 111408.
[13] Ranjbaran P, Yousefi H, Gharehpetian G B, et al. A review on floating photovoltaic (FPV) power generation units[J]. Renewable and Sustainable Energy Reviews, 2019, 110: 332-347.
[14] Cazzaniga R, Cicu M, Rosa-Clot M, et al. Floating photovoltaic plants: Performance analysis and design solutions[J]. Renewable and Sustainable Energy Reviews, 2018, 81: 1730-1741.
[15] Dai J, Zhang C, Lim H V, et al. Design and construction of floating modular photovoltaic system for water reservoirs[J]. Energy, 2020, 191: 116549.
[16] Liu H, Krishna V, Lun Leung J, et al. Field experience and performance analysis of floating

PV technologies in the tropics[J]. Progress in Photovoltaics: Research and Applications, 2018, 26(12): 957-967.

[17] Wang J, Lund P D. Review of recent offshore photovoltaics development[J]. Energies, 2022, 15(20): 7462.

[18] Song J, Kim J, Lee J, et al. Dynamic response of multiconnected floating solar panel systems with vertical cylinders[J]. Journal of Marine Science and Engineering, 2022, 10(2): 189.

[19] Lee J H, Paik K J, Lee S H, et al. Experimental and numerical study on the characteristics of motion and load for a floating solar power farm under regular waves[J]. Journal of Marine Science and Engineering, 2022, 10(5): 565.

[20] Jiang Z, Dai J, Saettone S, et al. Design and model test of a soft-connected lattice-structured floating solar photovoltaic concept for harsh offshore conditions[J]. Marine Structures, 2023, 90: 103426.

[21] Song J, Imani H, Yue J, et al. Hydrodynamic Characteristics of Floating Photovoltaic Systems under Ocean Loads[J]. Journal of Marine Science and Engineering, 2023, 11(9): 1813.

[22] Zhang D, Du J, Yuan Z, et al. Motion characteristics of large arrays of modularized floating bodies with hinge connections[J]. Physics of Fluids, 2023, 35(7).

[23] Noad, I. F., and R. Porter. "Modelling an articulated raft wave energy converter." Renewable Energy 2017, 114: 1146-1159.

[24] Zhao, X., Xue, R., Geng, J., & Göteman, M. Analytical investigation on the hydrodynamic performance of a multi-pontoon breakwater-WEC system. Ocean Engineering, 2021, 220: 108394.

[25] Li Z, Chen D, Feng X, et al. Hydroelastic analysis and structural design of a modular floating structure applying ultra-high performance fiber-reinforced concrete[J]. Ocean Engineering, 2023, 277: 114266.

[26] Zhang C, Wang P, Huang L, et al. Resonance mechanism of hydroelastic response of multi-patch floating photovoltaic structure in water waves over stepped seabed[J]. Physics of Fluids, 2023, 35(10).

[27] Tay Z Y. Three-Dimensional Hydroelasticity of Multi-Connected Modular Offshore Floating Solar Photovoltaic Farm[J]. Journal of Marine Science and Engineering, 2023, 11(10): 1968.

[28] Song J, Kim J, Chung W C, et al. Wave-induced structural response analysis of the supporting frames for multiconnected offshore floating photovoltaic units installed in the inner harbor[J]. Ocean Engineering, 2023, 271: 113812.

[29] Wei Y, Zou D, Zhang D, et al. Motion characteristics of a modularized floating solar farm in waves[J]. Physics of Fluids, 2024, 36(3).
[30] Zhu K, Shi H, Tao J, et al. Analytical study on hydrodynamic performance of co-located offshore wind–solar farms[J]. Physics of Fluids, 2024, 36(1).
[31] Zheng S M, Zhang Y H, Zhang Y L, et al. Numerical study on the dynamics of a two-raft wave energy conversion device[J]. Journal of Fluids and Structures, 2015, 58: 271-290.
[32] Liu C, Hu M, Zhao Z, et al. Latching control of a raft-type wave energy converter with a hydraulic power take-off system[J]. Ocean Engineering, 2021, 236: 109512.
[33] Zhou B, Huang X, Lin C, et al. Experimental study of a WEC array-floating breakwater hybrid system in multiple-degree-of-freedom motion[J]. Applied Energy, 2024 2024, 371: 123694.
[34] Zhou B, Lin C, Huang X, et al. Experimental study on the hydrodynamic performance of a multi-DOF WEC-type floating breakwater[J]. Renewable and Sustainable Energy Reviews, 2024, 202: 114694.
[35] Zhou B, Zheng Z, Zhang Q, et al. Wave attenuation and amplification by an abreast pair of floating parabolic breakwaters[J]. Energy, 2023, 271: 127077.
[36] Zhou B, Zheng Z, Hu J, et al. Annual performance and dynamic characteristics of a hybrid wind-wave floating energy system at a localized site in the North Sea[J]. Ocean Engineering, 2023, 280: 114872.
[37] Teng B, Taylor R E. New higher-order boundary element methods for wave diffraction/radiation[J]. *Applied Ocean Research*, 1995, 17(2): 71-77.
[38] Hu J, Zhou B, Vogel C, et al. Optimal design and performance analysis of a hybrid system combing a floating wind platform and wave energy converters[J]. *Applied energy*, 2020, 269: 114998.
[39] Zhou B, Zheng Z, Wang Y, et al. Optimization of an annular wave energy converter in a wind-wave hybrid system[J]. *Journal of Hydrodynamics*, 2023, 35(2): 338-350.
[40] Shabana A A. Dynamics of multibody systems[M]. Cambridge university press, 2020.
[41] Cummins W E. The impulse response function and ship motions[J]. Schiffstechnik, 1962, 9: 101-109.
[42] Liu, Y. A Coupled Approach for Dynamic Modelling of a Semi-submersible Type Platform with Multiple Diffuser-Augmented Wind Turbines (Doctoral dissertation, Kyushu University), 2015.
[43] Yu S R, Zhang M, Zhang D Q, et al. Optimal declutching control of hinged multiple floating bodies[J]. Ocean Engineering, 2024, 306: 117992.
[44] Chen M, Ouyang M, Guo H, et al. A coupled hydrodynamic–structural model for flexible

interconnected multiple floating bodies[J]. *Journal of Marine Science and Engineering*, 2023, 11(4): 813.

[45] Kim H S, Kim B W, Won Y, et al. Experimental Study on Structural Responses of Floating Photovoltaic System with Numerous Buoys and Connection Beams[C]//OCEANS 2021: San Diego–Porto. IEEE, 2021: 1-8.

[46] Zhang H, Zhou B, Zang J, et al. Optimization of a three-dimensional hybrid system combining a floating breakwater and a wave energy converter array[J]. Energy Conversion and Management, 2021, 247: 114717.

[47] Padovan A, Del Col D. Measurement and modeling of solar irradiance components on horizontal and tilted planes[J]. Solar Energy, 2010, 84(12): 2068-2084.

[48] Si Y, Chen Z, Zeng W, et al. The influence of power-take-off control on the dynamic response and power output of combined semi-submersible floating wind turbine and point-absorber wave energy converters[J]. Ocean Engineering, 2021, 227: 108835.

[49] Jin P, Zheng Z, Zhou Z, et al. Optimization and evaluation of a semi-submersible wind turbine and oscillating body wave energy converters hybrid system[J]. Energy, 2023, 282: 128889.

[50] Maghami M R, Hizam H, Gomes C, et al. Power loss due to soiling on solar panel: A review[J]. Renewable and Sustainable Energy Reviews, 2016, 59: 1307-1316.

Motion response and energy harvesting of multi-module floating photovoltaics in seas

Zheng, Zhi

2024-10-15

Zheng Z, Jin P, Huang Q, et al., (2024) Motion response and energy harvesting of multi-module floating photovoltaics in seas. Ocean Engineering, Volume 310, Part 2, October 2024, Article number 118760

https://doi.org/10.1016/j.oceaneng.2024.118760